Contribution of Sacrificial Anode in reinforced concrete patch repair: Results of numerical simulations

Eric Lozinguez, Jean-François Barthélémy, Véronique Bouteiller, Tiffany Desbois

Contribution of Sacrificial Anode in reinforced concrete Patch Repair: results of numerical simulations

Eric Lozinguez[a,*], Jean-François Barthélémy[a], Véronique Bouteiller[b], Tiffany Desbois[c]

[a] *Cerema, Project-team DIMA, 110 rue de Paris, BP 214, 77487 Provins Cedex, France*
[b] *Université Paris-Est, MAST, EMGCU, IFSTTAR,77447 Marne-la-vallée, France*
[c] *Cerema, Direction Ouest, 5 rue Jules Vallès, 22015 Saint-Brieuc Cedex, France*

Abstract

This paper deals with the numerical determination of potential and current distribution along the reinforcement when using patch repair applied to reinforced concrete elements. Numerical finite element models of the electrochemical phenomena demonstrate the useful contribution of Sacrificial Anode in improving the Cathodic Protection of the reinforcement by testing several configurations. The main result is that the Sacrificial Anode should be embedded in the substrate concrete area rather than in the patch area. Moreover, the influence of the resistivity of the repairing concrete is evaluated.

Keywords: Reinforded Concrete, Modelling studies, Patch repair, Sacrificial Anode for Cathodic Protection, Micro and Macro-cell corrosion

1. Introduction

Corrosion of the reinforcement is recognised as the main degradation of reinforced concrete structures [1]. From the point of view of service life, Tuutti, proposed a schematic sketch of steel corrosion sequence in concrete subdivided into an initiation stage and a propagation stage [2]. In the initiation stage, the aggressive species penetrate the concrete cover (carbonation reaction or chloride ion ingress) and once the rebar level is affected corrosion occurs and the propagation stage begins. Due to the diffusion/precipitation of the corrosion products and because the volume of iron corrosion products are higher than the volume of iron metal (2-6), disorders such as rust stains, cracks or spallings can be encountered.

According to the analysis of the questionnaires of the European CONREPNET Project [3], from the 230 case histories (main types of structures were buildings, bridges, dams, power stations and car parks), corrosion was the most common process of deterioration, being responsible for 55% of the problems. Patching was the most applied repair type (60% of the case histories) and after removing the defective concrete, the material used for the patching was "cementitious" type for 60%. Concerning the performance of repair, cementitious patches were 45% successful due to insufficient defective concrete having been removed and incipient anodes becoming dominant.

Therefore, recurring corrosion after patch repair could initiate in one of the three following areas: the patch area, the substrate (adjacent unrepaired area) or the interface between them [4, 5, 6, 7]. On the one hand, total or partial removal of contaminated concrete around the steel reinforcement will lead to two different situations: if the contaminated concrete is totally removed, corrosion damage will appear most likely within the substrate in the vicinity of the patch [8, 9] whereas if the contaminated concrete is only partially removed , the patch repair will more likely be deteriorated because of the creation of a macrocell between the top and the bottom of the steel and the subsequent development of rust below the rebar as schematized in Fig. 1 (3D view visible in the foreground of Fig. 22). On the other hand, incipient anode will consist in macrocell corrosion [10, 11, 12, 13, 14, 15, 16, 17, 18, 19] resulting from treated and not treated areas.

*Principal corresponding author
Email addresses: eric.lozinguez@cerema.fr (Eric Lozinguez), jean-francois.barthelemy@cerema.fr (Jean-François Barthélémy), veronique.bouteiller@ifsttar.fr (Véronique Bouteiller), tiffany.desbois@cerema.fr (Tiffany Desbois)

At the scale of the structure, it is worth recalling that the main difference between microcell and macrocell corrosion lies in the fact that the anodic and cathodic reactions take place at the same location for the former and at different locations for the latter, creating thus a ionic current within concrete.

Even if the removal of the contaminated concrete is complete and the alkalinity of the new concrete is supposed to protect the reinforcement from corrosion, experience shows that patch repair rarely exceeds the 10-year guarantee [20].

In order to reduce this recurring corrosion, the use of Sacrificial Anode for Cathodic Protection (SACP) embedded into the concrete seems an attractive solution. Indeed this technique takes advantage of the electrochemical properties of zinc which, as a less noble metal than iron, corrodes preferably and consequently protects the neighbouring rebars. This protection technique has been used for decades in civil engineering as well as in the maritime field and some feedbacks on protected structures can be found [21, 22, 23, 24, 25]. In literature, few articles tackle the issue of the efficiency of SACP in patch repair and the feedbacks on structures do generally not give much details about the precise locations of the anodes. Christodoulou's study focused on the arrangement of galvanic anodes for the repair of reinforced concrete structures and highlighted that anodes had a dominant effect on potentials to a distance between 250 and 600 mm [26]. Soleimani modelled the kinetics of corrosion and found that resistivities of the patch repair and that of substrate concretes were the most significant factors affecting the corrosion that occurred mainly in the 2-5 cm portion of interface between them [9]. Cheung modelled the electrochemical corrosion process with SACP by means of 2D numerical simulations and found that the location of the anode in the substrate rather than in the patch area lead to significant reduction of the macrocell corrosion [27]. For patch repair of RC structures, Qian studied both components (microcell and macrocell) of corrosion from theoretical and experimental work [10]. Ribeiro proposed a criterion, based on experimentals results, to prevent the macrocell corrosion inside patch repairs based on the least electrochemical incompatibility between patch repair and substrate concretes in the case of corrosion induced by carbonation [28].

This paper presents the results of numerical simulations used to evaluate the efficiency of the SACP in patch repair. Eight cases are studied considering two repair situations (anodic area with total removal of contaminated concrete around the reinforcement on a limited longitudinal extension or cathodic area and partial removal of the contaminated concrete around the rebar) and four conditions: one before repair and three after repair without SACP, with SACP in the patch repair and with SACP in the substrate. Moreover the resistivity of the repairing concrete is also evaluated. These numerical results (mainly potential and current distributions) are very helpful as experimental work on this issue is scarce because rather difficult or impossible to be conducted. In addition, the use of 3D finite elements models and related softwares help illustrating and quantifying the reduction in corrosion that causes the sacrificial anode.

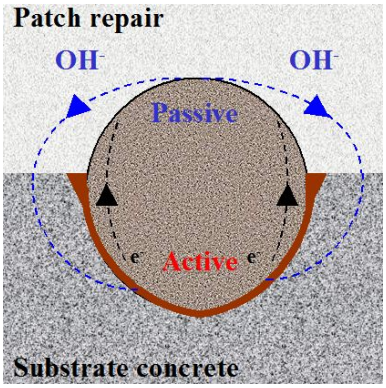

Figure 1: Illustration of macrocell corrosion around the steel

2. Presentation of the work

2.1. Case studies and associated corrosions

2.1.1. Case studies

When dealing with patch repair, several scenarii may occur. In this study, eight case studies are considered based on two situations that are subdivided into four conditions. The first situation refers to a repair where the contaminated concrete around the reinforcement is totally removed but the vicinity of the repaired area is still an anodic area (the concrete is still adhesive but is contaminated). For the second situation, the contaminated concrete around the reinforcement is only partially removed but the vicinity of the repaired area is not contaminated. The four conditions considered are:

- before repair;
- after repair, without SACP;
- after repair, with SACP embedded in the patch repair;
- after repair, with SACP embedded in the susbstrate (adjacent unrepaired area).

2.1.2. Corrosion associated to the first situation

For the first situation and before repair (Fig. 2), the entire length of the steel rebar is corroding (as the concrete is contaminated) and the resulting corrosion is of microcell type. This means that cathodic and anodic areas are merged: there is no macroscopic movement (at the scale of the studied reinforced concrete area) of electrons (along the steel) or ions (through the concrete pore solution). Corrosion of steel results from two simultaneous half-cell reactions:

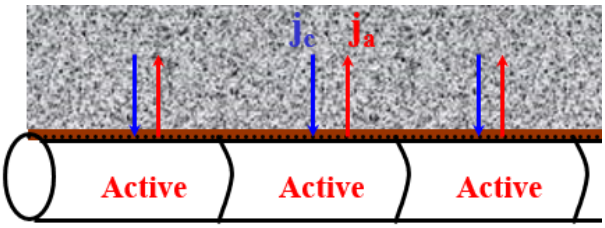

Figure 2: Situation 1 - Microcell before patch repair

- the anodic reaction corresponding to the oxidation of iron creates a current density $j_{a,micro}$ considered positively outward from the steel rebar;

$$Fe \rightarrow Fe^{2+} + 2e^{-} \tag{1}$$

- the cathodic reaction corresponding to the reduction of oxygen in the presence of water creates a current density $j_{c,micro}$ considered positively inward to the steel rebar;

$$2H_2O + O_2 + 4e^{-} \rightarrow 4OH^{-} \tag{2}$$

In microcell corrosion, for any point distributed along the steel/concrete interface, $j_{a,micro} = j_{c,micro}$.

After patch repair, macrocell corrosion occurs as illustrated in Fig. 3. Electrical and ionic currents appear respectively in steel and concrete and j_a becomes different from j_c:

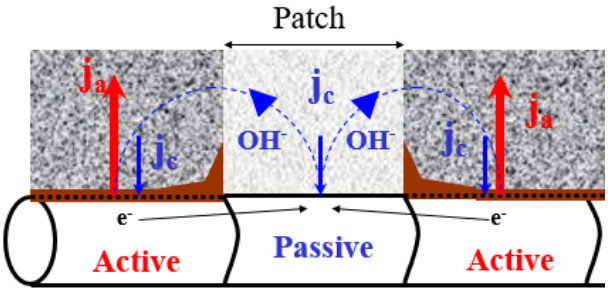

Figure 3: Situation 1 - Macrocell after patch repair

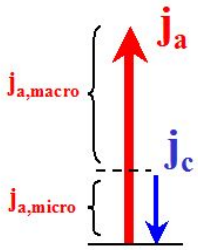

Figure 4: Microcell and macrocell current densities

- in active areas, the resulting anodic current corresponding to the iron oxydation, j_a, is the sum of the micro and macro cell currents as illustrated in Fig. 4;
- in passive areas, only one current density corresponding to the reduction of oxygen dissolved in water, j_c, is considered (the anodic current is so low that it can be neglected).

2.1.3. Corrosion associated to the second situation

The second case that is considered consists in a well-sized patch but with contaminated concrete not fully removed around the rebar as illustrated in Fig. 5 (cross section is given in Fig. 1). It is assumed that only half of the circumference of the steel is active after repair.

Before repair (at the top of Fig. 5), macrocell corrosion is already present between the contaminated concrete (concrete whose upper part will be replaced by the patch repair) and the sound concrete (substrate concrete).

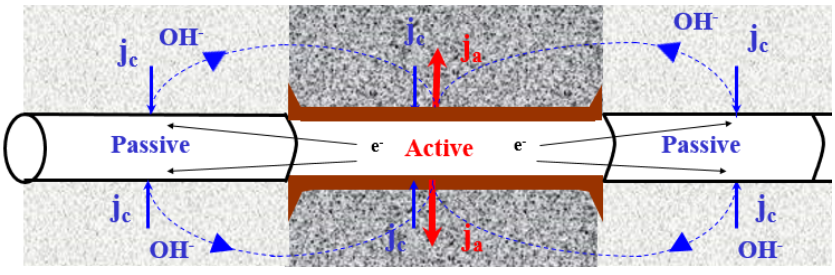

Figure 5: Situation 2 - Before patch repair

After repair (at the bottom of Fig. 6), the upper part of the steel becomes a passive region: the anodic/cathodic surfaces ratio decreases, which increases the macrocell corrosion under the rebar.

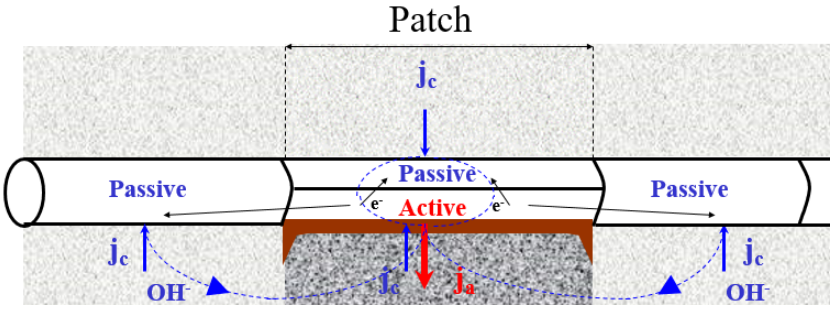

Figure 6: Situation 2 - After patch repair

2.2. *Geometry of the reinforced concrete element to be repaired*

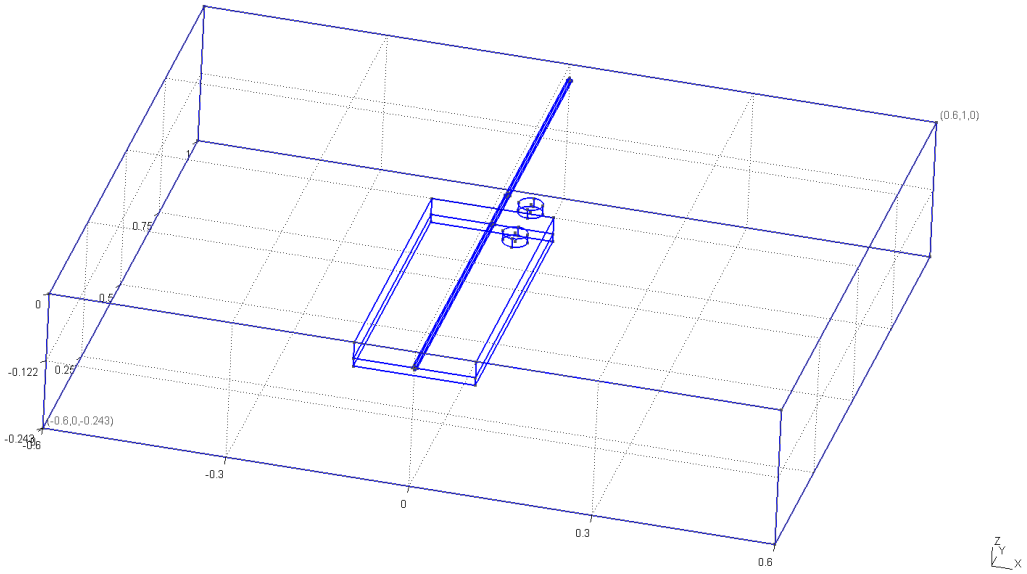

Figure 7: Patch repair geometry (distances in meters)

For reasons of symmetry, half of the patch is considered in the model.

As illustrated in Fig. 7, the geometry of the reinforced concrete to be repaired is considered as a rectangular parallelepiped with total dimensions of 100 cm width, 120 cm length and 24,3 cm thickness. Inside this box, the geometry of the patch area is rectangular (50 cm wide and 20 cm long): 4.3 cm thick in case 1 while in case 2 only 2.9 thick. The diameter of the steel reinforcement is equal to 8 mm. The concrete cover is chosen equal to 25 mm (for civil engineering bridges the concrete cover is generally around 30 mm but for buildings a concrete cover of 10 mm is often encountered).

The cylindrical SACP has a radius of 20 mm and a length of 15 mm. It is covered by 10 mm of concrete and its center is positioned at a distance of 50 mm from the rebar axis and 50 mm from the patch/substrate interface. Depending on the conditions, none or only one of the anodes (either in the patch or in the substrate) is active.

In reinforced concrete structures, steel rebars are arranged as a mat or cage with several layers connected [29]. The proposed finite element model does not take into account the rebar mesh distribution even if technically it would not be a problem. Only one bar is considered in this $3D$ problem in order to simplify the interpretation of the results and

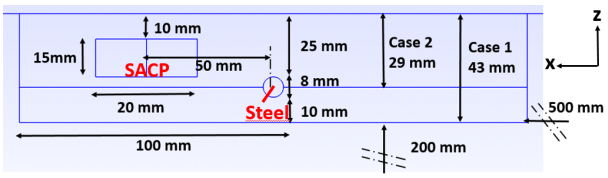

Figure 8: Geometry zoom in patch repair (XZ plan w.r.t Fig. 7)

to highlight the practice drawbacks observed on site (small patch repair area or contaminated concrete not completely removed around the steel). Finally taking into account a complete mesh would reduce the anodic/cathodic ratio and thus increase the corrosion current but the influence of the remote rebars on the macrocell current is expected to be lower than that of the cathodic zone in the immediate vicinity of the corroding area.

Detailed features of geometry depending on the repair situation are presented in Fig. 8.

For the first situation, the patch depth is extended by 10 mm (the patch depth is 43 mm and substrate concrete exceeds by 20 cm). For the second situation, the bottom of the patch is located at a depth of 29 mm (concrete cover in addition with a half diameter of the rebar) and substrate concrete exceeds by 21,4 cm.

3. Description of the numerical model

3.1. Numerical model of corrosion

This section aims at presenting the numerical procedure allowing to build the solution of a corrosion problem from the electrochemical point of view. A major hypothesis is that the active and passive steel zones, resulting from the incubation process, are known in the model although they can be very difficult to identify from measurements [30, 31, 32].
The studied domain here is the space occupied by the concrete. The electrochemical reactions responsible for corrosion are written at the concrete/steel interface where the so-called electrode potential E, which controls the corrosion, is defined as [33]:

$$E = \Phi_M - \Phi_S \tag{3}$$

Where Φ_M is the potential of the metal and Φ_S that of the neighbouring electrolyte.

Hence E actually appears as a potential jump across the concrete/steel interface. Since the potential field is defined up to an arbitrary constant and can be considered as constant within steel due to the high conductivity of the latter with respect to concrete, it is proposed to choose $\Phi_M = 0$ in the following.
With the constant previously chosen, Eq. (3) simplifies:

$$E = -\Phi_S \tag{4}$$

Thus the field E defined at the steel/concrete interface depends on the location along and around the rebar through Φ_S

3.1.1. Equation in concrete

From the electrical point of view, concrete is considered here as an ohmic conductor owing its conductivity to its microstructure and the degree of saturation of the interstital solution as well as the conductive property of the latter. The macroscopic ohm's law and the local charge conservation leads to the following elliptic equation:

$$\mathrm{div}(-\frac{1}{\rho}\mathbf{grad}\Phi_s) = 0 \tag{5}$$

with:
Φ_s: scalar field of potential in the solution (V/ESH);
ρ: scalar field of electrical resistivity ($\Omega.m$).

3.1.2. Boundary conditions

The anodic and cathodic current densities are related to the electrode potential by the classical polarization equations [14]:

- For active steel:

$$\mathbf{j}.\mathbf{n} = -j^0_{a,Fe}\exp\frac{\ln(10)(-\Phi_S - E^{eq}_{Fe})}{\beta_{a,Fe}} + j^0_{c,O_2/Fe}\exp\frac{\ln(10)(E^{eq}_{O_2} + \Phi_S)}{\beta_{c,O_2/Fe}} \tag{6}$$

- For passive steel:

$$\mathbf{j}.\mathbf{n} = j^0_{c,O_2/Fe}\exp\frac{\ln(10)(E^{eq}_{O_2} + \Phi_s)}{\beta_{c,O_2/Fe}} \tag{7}$$

with:
$\boldsymbol{j}$: vector current density ($A.m^{-2}$);
$\mathbf{n}$: outward unit normal to the concrete domain;
$j^0_{a,Fe}$: anodic exchange current density ($A.m^{-2}$);

$j^0_{c,O_2/Fe}$: cathodic exchange current density ($A.m^{-2}$);
E^{eq}_{Fe}: iron equilibrium potential ($Vvs.SCE$);
$E^{eq}_{O_2}$: oxygen equilibrium potential ($Vvs.SCE$);
$\beta_{a,Fe}$: anodic iron Tafel slope (V/dec);
$\beta_{c,O_2/Fe}$: cathodic oxygen (/iron) Tafel slope (V/dec).

For all other boundaries of the model, there is no electrical transfer so Neumann conditions with zero flux apply:

$$\mathbf{j}.\mathbf{n} = -\frac{1}{\rho}\frac{\partial \Phi_s}{\partial n} = 0 \tag{8}$$

3.1.3. Taking into account SACP

The principle of sacrificial anodes lies in the fact that zinc is less noble than iron: so if they are electrically connected in the presence of an electrolyte, zinc will tend to corrode instead of steel. This galvanic protection is a method based on the Mixed-Potential Theory [34].

At the interface of SACP two conditions are added:
A mixed condition in the same way as for steel;

$$\mathbf{j}.\mathbf{n} = -j^0_{a,Zn}\exp\frac{\ln(10)(-\Phi_s - E^{eq}_{Zn})}{\beta_{a,Zn}} + j^0_{c,O_2/Zn}\exp\frac{\ln(10)(E^{eq}_{O_2} + \Phi_s)}{\beta_{c,O_2/Zn}} \tag{9}$$

with:
$j^0_{a,Zn}$: anodic exchange current density ($A.m^{-2}$);
$j^0_{c,O_2/Zn}$: cathodic exchange current density ($A.m^{-2}$);
E^{eq}_{Zn}: zinc equilibrium potential ($Vvs.SCE$);
$E^{eq}_{O_2}$: oxygen equilibrium potential ($Vvs.SCE$);
$\beta_{a,Zn}$: anodic zinc Tafel slope (V/dec);
$\beta_{c,O_2/Zn}$: cathodic oxygen (/zinc) Tafel slope (V/dec);

3.2. Model parameters

Electrochemical input data for this study (gathered in Tab. 1 ,polarization curves are plotted in Fig. 9) are chosen from literature [35, 18] although dispersions have already been highlighted [36]. The equilibrium potential and the Tafel slopes are not so dispersed but the values of exchange current densities may be very different according to the authors. These dispersions can be explained by the state of the steel/concrete interface, the ionic content of the interstitial solution and finally the relative humidity and temperature conditions. Quantitative results of numerical simulations may of course depend on the chosen input data but preliminary results of parametric studies show that the qualitative conclusions drawn in this parer remain valid.

3.3. Influence of concrete resistivity

To determine the efficiency of patch repair, the resistivity of concretes (substrate as well as patch) is still an important issue. In this study, the electrical resistivity for substrate concrete is kept equal to 100 $\Omega.m$. The electrical resistivity of the patch concrete is studied as a parameter and varied from 50 to 1400 $\Omega.m$ according to values from literature [14, 37, 38, 32]. The 200 $\Omega.m$ value complies with the ISO EN 12696 standard [39] and is presented in detail. On-site, patch concrete (or repair mortar) can be reinforced and in this case, high values such as 1400 $\Omega.m$ can be found.

	Parameter	Symbol	Selected Value	Unit
Fe	Anodic equilibrium potential	E^{eq}_{Fe}	-0.680	$Vvs.SCE$
	Anodic exchange current density	$j^0_{a,Fe}$	100.10^{-6}	$A.m^{-2}$
	Anodic Tafel slope	$\beta_{a,Fe}$	90.10^{-3}	V/dec
Oxygen on Fe	Cathodic equilibrium potential	$E^{eq}_{O_2}$	0.160	$Vvs.SCE$
	Cathodic exchange current density	$j^0_{c,O_2/Fe}$	6.10^{-6}	$A.m^{-2}$
	Cathodic Tafel slope	$\beta_{c,O_2/Fe}$	180.10^{-3}	V/dec
Zn	Anodic equilibrium potential	E^{eq}_{Zn}	-1.050	$Vvs.SCE$
	Anodic exchange current density	$j^0_{a,Zn}$	16.10^{-6}	$A.m^{-2}$
	Anodic Tafel slope	$\beta_{a,Zn}$	60.10^{-3}	V/dec
Oxygen on Zn	Cathodic exchange current density	$j^0_{c,O_2/Zn}$	2.10^{-6}	$A.m^{-2}$
	Cathodic Tafel slope	$\beta_{c,O_2/Zn}$	180.10^{-3}	V/dec

Table 1: Electrochemical parameters

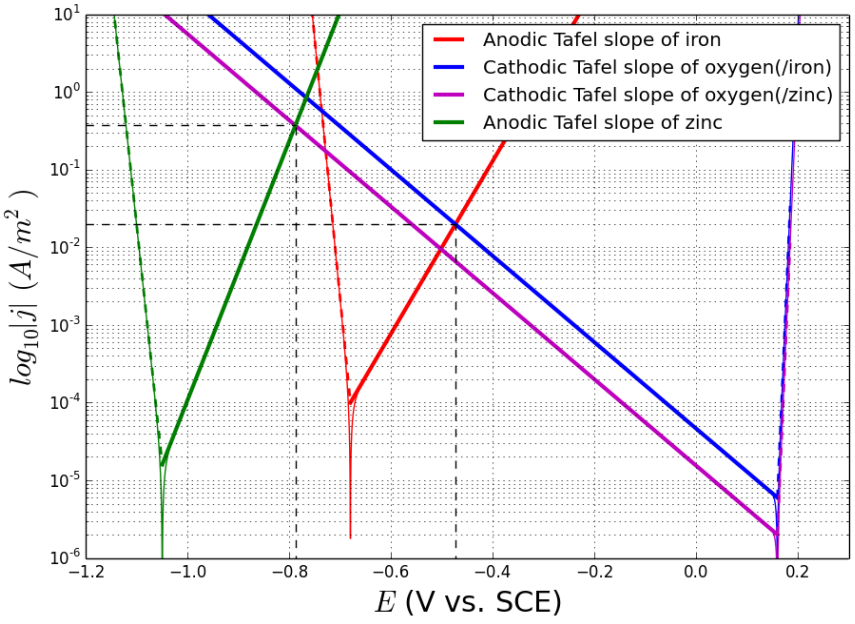

Figure 9: Polarization curves of iron and zinc with electrochemical parameters in Tab. 1

4. Results of numerical simulations

Numerical simulations of corrosion have been recently presented in the literature [36, 14, 15, 40]. In this paper, Finite Element Method (FEM) is used with the free software GetFEM++ [41], GMSH for the mesh [42] and Paraview [43]. By means of very efficient generic elementary tools, GetFEM++ allows to build the solution to non-linear problems including those involving nonlinear boundary conditions (as Butler-Volmer equation). It also offers the possibility to consider coupled (e.g. electrochemical problem coupled with oxygen diffusion) as well as non-stationary problems (e.g. induced by the capacitive effect of the double layer at steel/concrete interface). Such features are also available in commercial softwares such as Comsol Multiphysics [44] but GetFEM++ has the advantage to be free and open source, which makes it very accessible to the scientific community.

4.1. *Situation 1: total removal of contaminated concrete around the steel reinforcement in the patch area but adjacent area is still contaminated*

Potential and current distributions along the steel reinforcement in the patch area (patch) and in the adjacent area (substrate) are presented in Fig. 10 and in Fig. 13 respectively. Before repair, the potential is uniform over the whole volume (i.e. microcell corrosion) and equal to -473.31 mV vs. SCE (Fig. 10) and the anodic current density (Fig. 13) is equal to 1.934 $\mu A.cm^{-2}$. Thus the calculated overall anodic current intensity along the steel reinforcement of one meter length is 486.06 μA.

After patch repair, 50 cm of the reinforcement is considered passive (in the patch area because the contaminated concrete has been totally removed) and 50 cm of the reinforcement is considered active (because the concrete adjacent to the repaired area remained contaminated). In this case macrocell corrosion occurs which results evolve depending on the conditions of SACP (without SACP, SACP in the patch or SACP in the substrate). In this study, the efficiency of the SACP is investigated.

4.1.1. *Potential distributions*

Potential distributions along the steel reinforcement in the adjacent area of the patch (substrate) presented in Fig. 10 shows different results:

- the potential after repair without SACP is less electronegative than before patch repair meaning that an increase of corrosion is achieved;
- the potential after repair with SACP is more electronegative than before patch repair as expected in a Cathodic Protection process. Results also highlight that a SACP embedded in the substrate concrete rather than in the patch concrete induces a better efficiency of the Cathodic Protection.

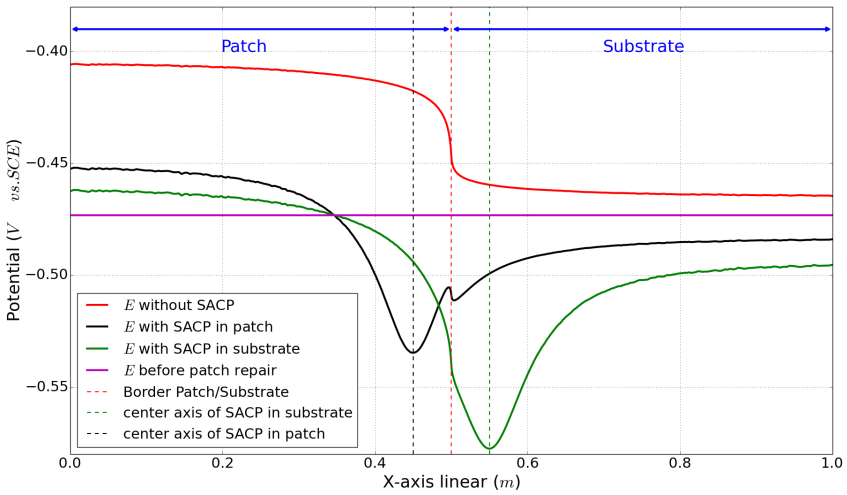

Figure 10: Situation 1 - Potential distributions along the steel reinforcement in the patch area (patch) and in the adjacent area (substrate) ($V vs. SCE$)

In order to evaluate the efficiency of the CP obtained with SACP, the depolarisation values (difference of potentials without SACP and with SACP) are presented in Figure 11 together with the 100 mV protection criterion for Impressed Current Cathodic Protection (ICCP) as described in the ISO 12696 standard [39]. Results show that whatever the position of the sacrificial anode (in the patch or in the substrate), the criterion of 100 mV is achieved but over a rather small distance ($\simeq$ 15 cm) which does not even reach the active part of steel in the case of SACP in patch. This information is useful for field trials, first, to correctly design the protection and, second to determine the position of the embedded reference electrode on which is based the monitoring.

To go further in this optimization approach, numerical simulations of the potential distribution around the rebar depending on the angle with the anode are illustrated in Fig. 12. Depending on whether it is in front or opposite of SACP, this mask or screen effect can vary the potential from more than 30 mV. Moreover, it appeares that the potential distribution is strongly influenced by the angle, within a 20 cm area. This behaviour will also play an important role in the determination of the depolarisation value. As expected, when the distance increases this effect fades.

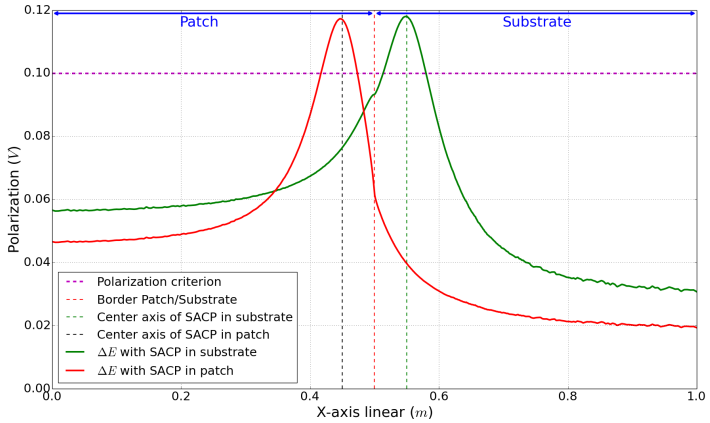

Figure 11: Situation 1 - Depolarisation values obtained with SACP embedded in the patch or in the substrate and criterion of efficiency for ICCP [39] (in dotted line)

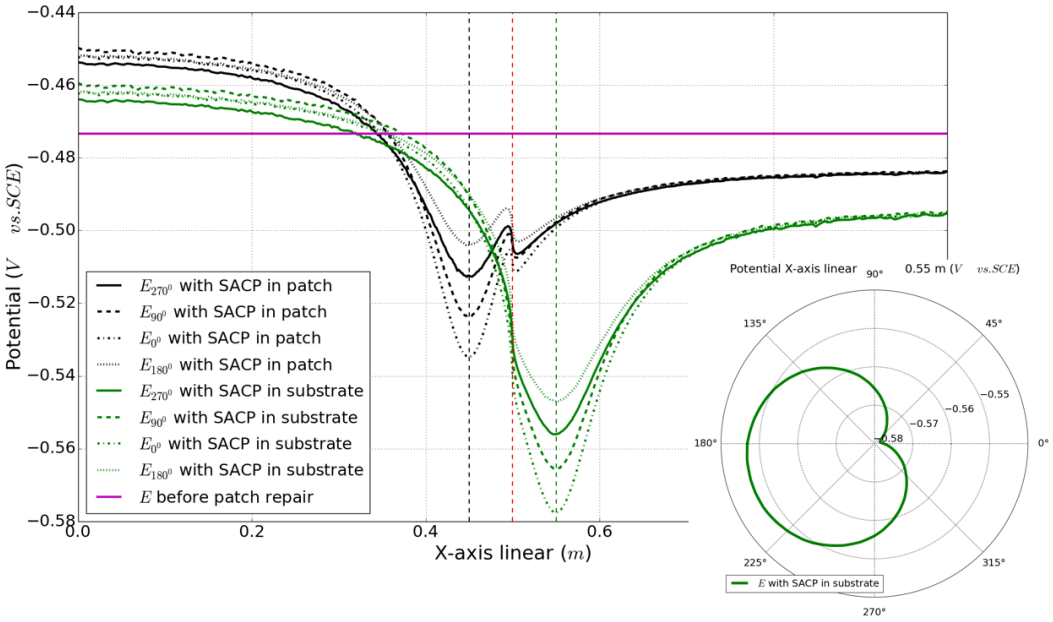

Figure 12: Situation 1 - Potential distributions along the steel reinforcement and around the steel reinforcement (bottom right) depending on the angle

Case	Current intensity	Patch	Substrate	SACP
Before repair	I_c	243.03	243.03	-
	$I_a - I_c$	0.0	0.0	-
	I_a	243.03	243.03	-
Without SACP	I_c	109.70	214.23	-
	$I_a - I_c$	-	109.70	-
	I_a	-	323.94	-
SACP in Patch	I_c	246.12	299.52	1874.32
	$I_a - I_c$	-	-131.54	377.67
	I_a	-	167.97	2251.99
SACP in Substrate	I_c	246.83	428.82	1835.93
	$I_a - I_c$	-	-329.01	575.85
	I_a	-	99.81	2411.78

Table 2: Situation 1 – Current calculations in μA (patch concrete resistivity is equal to 200 $\Omega.m$, substrate concrete resistivity is equal to 100 $\Omega.m$)

4.1.2. Current density distribution

Current density distributions along the steel reinforcement in the adjacent area of the patch (substrate) presented in Fig. 13 contribute to different observations:

- before repair, the current density along the steel is equal to 2 $\mu A.cm^{-2}$ and is constant;
- after repair without SACP, a macrocell anodic current density occurred in substrate because the rebar remaines in a contaminated concrete;
- after repair with SACP, some of the corrosion of the rebar (still in a contaminated medium) is inhibited. The efficiency of the protection is improved when the SACP is embedded in the substrate rather than in the patch.

As shown on the top right of Fig. 13 current protection has a spatial effect: the current still present at 0.55m is double in backside as compared to the side in front of SACP. For a single layer of reinforcement in typical conditions, the surface of a steel bar facing the anode may receive 1.5 times the current received by the opposite surface.

Table 2 gathers the figures of the currents calculated as the integrals of current densities of the steel reinforcement located in the 50 cm of patch concrete and in the 50 cm of substrate concrete. It can be observed that:

- after patch repair without SACP, the corrosion of the steel in the substrate (adjacent to the repaired area) is increased by 33 %. This result is well known on-site where the degradations of the reinforced concrete appear at the vicinity of the repaired one after some years;
- after patch repair with SACP, the Ia-Ic values are negative, which likely means that only microcell current remaines (no macrocell). Moreover the contribution of the CP is quantified with a decrease of current by 48% and 69% respectively for SACP located in the patch or in the substrate. This latter case is more efficient because, first, the steel is corroding only in the contaminated substrate (steel in the patch area became passive) and, second, because the distance between the reinforcement and the substrate anode is smallest. Futhermore the relatively high electrical resistivity of patch concrete (*i.e.* 200 vs. 100 $\Omega.m$) prevents the sacrificial anode from properly disseminating its protective current.

Table 2 represents the global intensity: for example, current as 167.97 μA (resp. 99.81 μA) corresponds to an average density current at 1.34 $\mu A.cm^{-2}$ (resp. 0.79 $\mu A.cm^{-2}$) but macrocell corrosions create a non-uniformity of the current density. The finite element solution allows building the field of current density and more particulary the anodic one at the interface between active steel and concrete directly related to the oxidation of steel and material loss (area where corrosion peaks are observed).

With the SACP in substrate, self-corrosion of the zinc (i.e. microcell) is about 1836μA to which is added 576μA of macrocell totaling 2412μA of zinc consumption: this current reduces 224μA of steel corrosion in substrate concrete. The yield is close to 10%

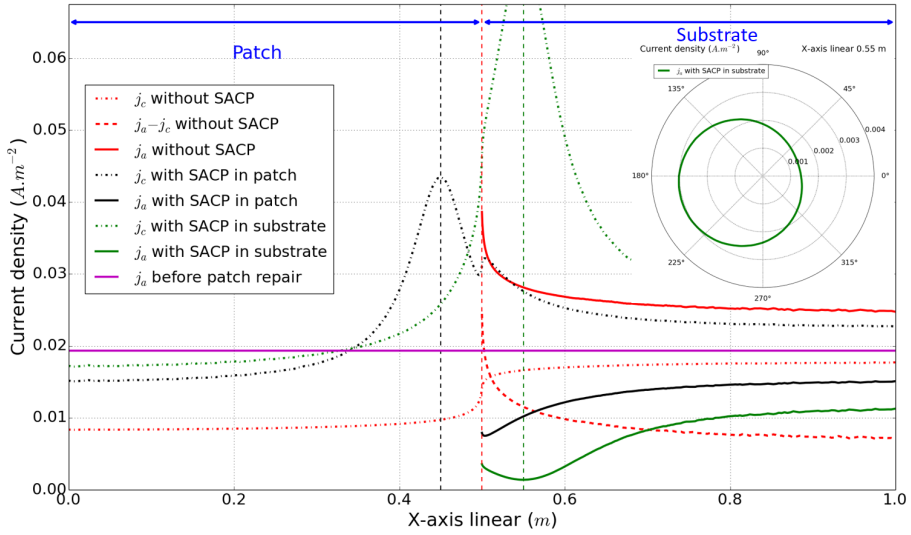

Figure 13: Situation 1 - Current distributions along the steel reinforcement in the patch area (patch) and in the adjacent area (substrate)

The previous findings can be visually observed on Fig. 14 which illustrates the 3D Finite Element Model results representing the potentials and the field lines (current) depending on the tested conditions:

- before repair, there is no current field line as the potential is uniform;
- after repair without SACP, current field lines appear between cathodic area (repaired area) and anodic area (substrate concrete which remain contaminated and therefore exhibit lower potentials);
- after repair with SACP, either in the patch or in the substrate, current field lines (from CP) were all over the steel reinforcement and no macrocell corrosion occurred between active and passive steel.

4.1.3. Effect of the electrical resistivity of the patch concrete

The resistivity of the patch concrete strongly impacts the current and therefore the efficiency of the treatment as represented in Fig. 15 which represents the global current on steel in the substrate. Before repair, the current is constant and equal to 240 μA. After Patch Repair without SACP, current increases (320 to 300 μA) with increasing resisitivity (50 to 1400 $\Omega.m$): Thus the repair increases the corrosion where contaminated concrete is still present (decrease of anodic /cathodic surfaces ratio). The position of the SACP strongly influences the current. When embedded in the patch, the current increases from 100 to 250 μA and for resistivities exceeding 1000 $\Omega.m$ the current became equal to the one before repair meaning that the SACP brought no improvement. When the SACP is embedded in the substrate, the current almost reaches a step (100 μA) 2.5 times lower than the one before repair meaning that the efficiency is improved.

For SACP in substrate concrete, the efficiency slightly increases because the electrical field lines are less dispersed in the patch where the protective current is not necessary (steel becomes passive in an alkaline environment).

4.2. Situation 2: partial removal of contaminated concrete around the steel reinforcement in the patch area and adjacent area is not contaminated

As in section 4.1, the electrical resistivity of patch repair is set to 200 $\Omega.m$: It will only vary in subsection 4.2.3.

Before the repair, macrocell corrosion is still present along the steel: the anode/cathode ratio decreases after the repair.

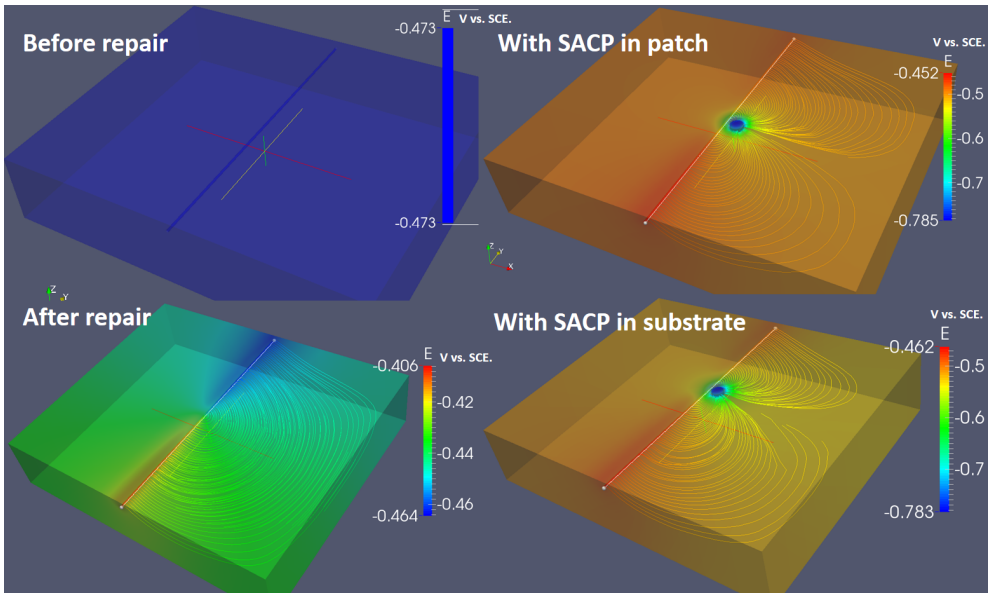

Figure 14: Situation 1 - 3D Finite Element Model simulating the potential and current distributions depending on the conditions (before repair and after repair considering no SACP, SACP in the patch and SACP in the substrate)

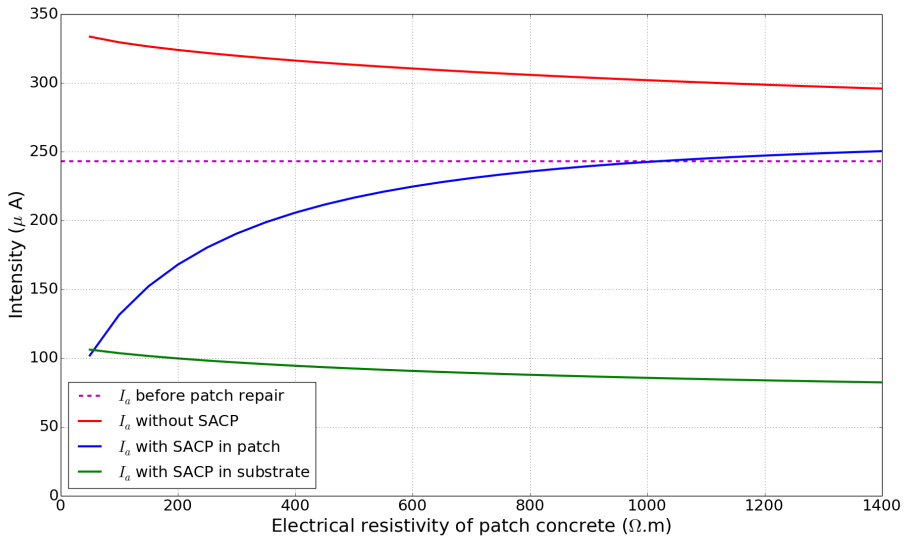

Figure 15: Situation 1 - Effect of the patch concrete resistivity on current (μA)

4.2.1. Potential distributions

Fig. 16 represents the potential along a line of the cylinder: this line is under the steel for this case. The corrosion is present only on the lower half of the cylinder (under the patch repair).

As regards the steel below the patch, the potential without SACP is upper than before patch repair: the repair has therefore deteriorated the existing situation for the active steel. At about an abscissa of 0.45 m, the potential with SACP in the patch is lower than the one with SACP in substrate but this is not the case further away from the abscissa

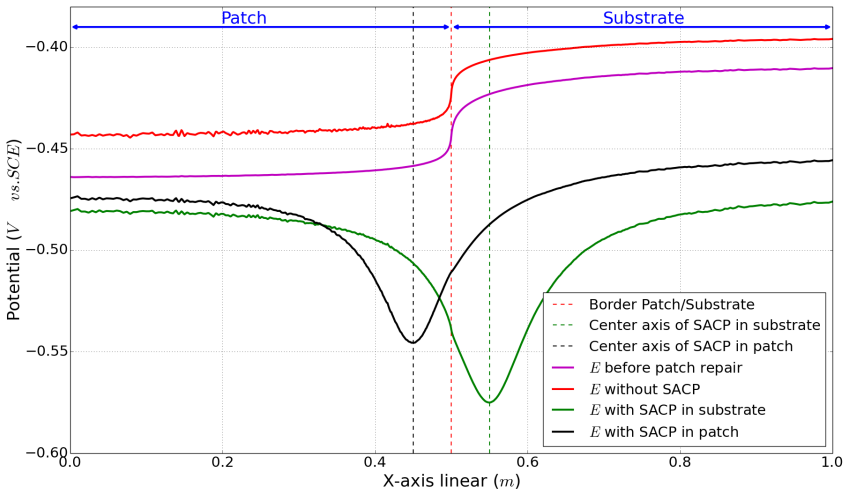

Figure 16: Situation 2 - Potential distribution along the steel reinforcement (V $vs.$ SCE)

of the SACP in the patch.

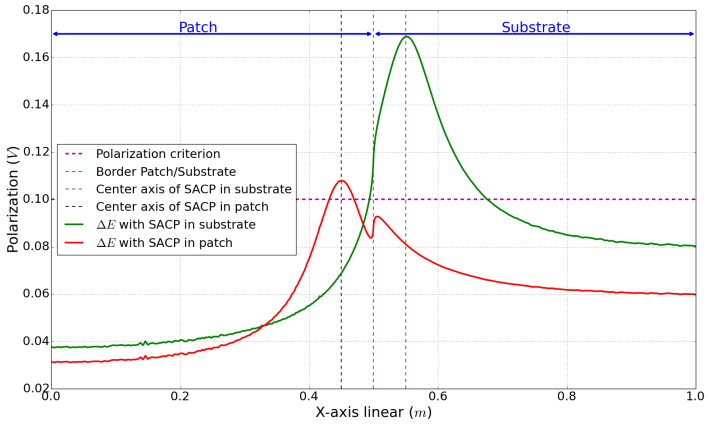

Figure 17: Situation 2 - Depolarisation values (V)

Fig. 17 shows that the depolarization criterion [39] is achieved only with SACP in patch and only on a very small range. With SACP in substrate concrete this criterion is only achieved in passive steel part but it is useless.

Fig. 18 evinces the evolution of the potential around the rebar against the angle: in front of SACP in patch (at 0.45m X-axis linear), the potential varies from more than 30 mV (as in case 1). Once again, the spatial distribution of protection must be taken into account.

4.2.2. Current density distributions

Tab.3 shows that:

- for the steel still active, the overall intensity increases by 53 % after the repair without SACP;

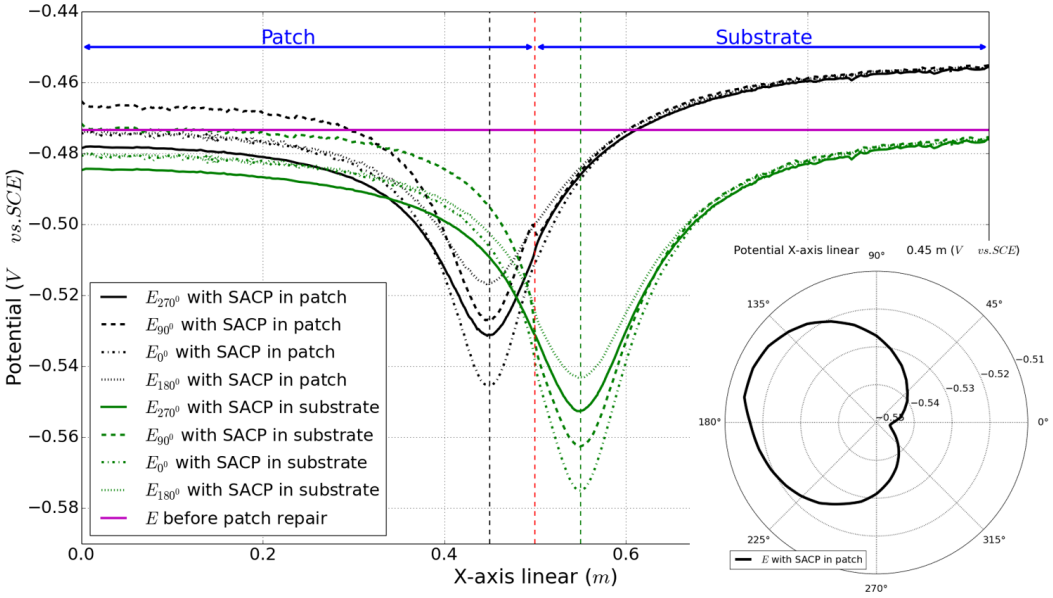

Figure 18: Situation 2 - Potential distributions along the steel reinforcement and around the steel reinforcement depending on the angle ($V\,vs.SCE$)

- with SACP in patch, the overall intensity drops by 67 % and with SACP in substrate by 69 %.

In both cases with SACP, the macrocell current (I_a-I_c) values are negatives (only microcell current is still present). With 200 $\Omega.m$ of electrical resistivity for the concrete patch, the two situations look very similar.

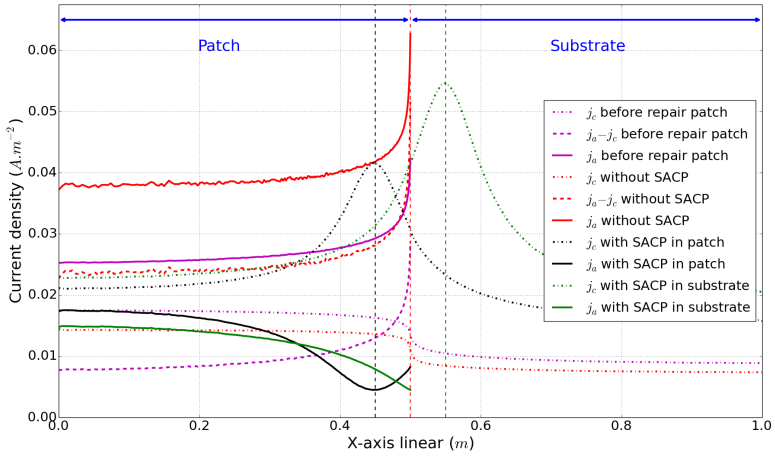

Figure 19: Situation 2 - Current densities along steel reinforcement ($A.m^{-2}$)

Fig 19 is established with a line representing the inferior part of the rebar: the solid curves corresponding to the oxydation of steel show that the SACP reduces the peak of corrosion at the interface patch/substrate.

Fig 20 illustrates the screen effect of current protection: it is less apparent with SACP in substrate because the anode is further away from the corroded zone at 0.45 m. In front of the SACP in patch the current is about 0.3

Case	Current intensity	Patch (up)	Substrate (below the patch)	Substrate	SACP
before repair	I_c	106.18	105.64	117.22	-
	$I_a - I_c$	57.49	59.73	-	-
	I_a	163.67	165.36	-	-
Without SACP	I_c	73.23	85.12	96.26	-
	$I_a - I_c$	-	169.48	-	-
	I_a	-	254.60	-	-
SACP in Patch	I_c	144.39	158.71	227.54	1860.93
	$I_a - I_c$	-	-74.09	-	446.02
	I_a	-	84.62	-	2306.95
SACP in Substrate	I_c	139.84	156.24	372.44	1833.53
	$I_a - I_c$	-	-76.62	-	588.90
	I_a	-	79.62	-	2422.43

Table 3: Situation 2 – Current calculations in μA (patch concrete resistivity is equal to 200 $\Omega.m$, substrate concrete resistivity is equal to 100 $\Omega.m$)

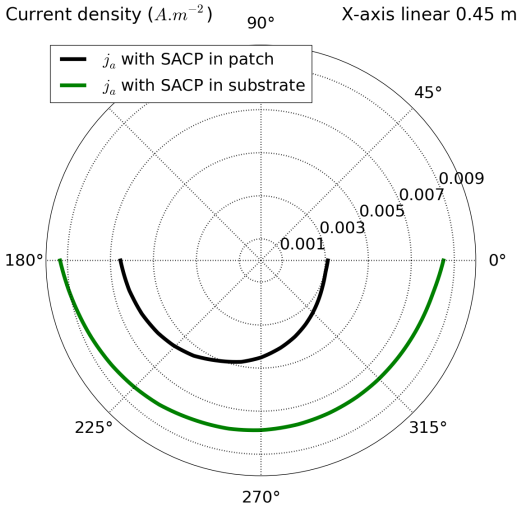

Figure 20: Situation 2 - Current distribution around the steel reinforcement depending on the angle ($A.m^{-2}$)

$\mu A.cm^{-2}$, while on the other side it is about 0.7 $\mu A.cm^{-2}$.

4.2.3. Effect of the electrical resistivity of the patch concrete

Fig 21 shows that 200 $\Omega.m$ approximately corresponds to the crossing of the two curves. The efficiency of the SACP in patch repair strongly decreases with the resistivity while it remains relatively independant of the resitivity of the patch when the SACP is located within the substrate.

Fig 22 is etablished with a resistivity at 1000 $\Omega.m$ and with SACP in patch: only a small portion of the steel is protected by the SACP and macrocell currents are visible with the field lines of circular shape between active (below) and passive (up) steel rebar.

5. Conclusions

All along the studied cases, it has been established that:

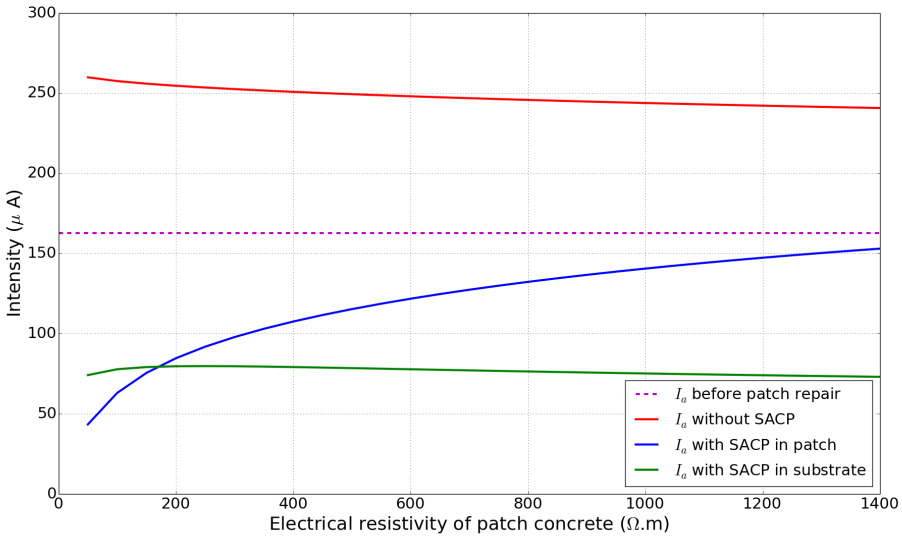

Figure 21: Situation 2 - Effect of the patch concrete resistivity on current (μA)

- patch repair always leads to corrosion increase of the active steel within the remaining substrate concrete: hence it is necessary to optimize the length of the repair as well as the position of the anodes;
- it is preferable to place the SACP in the substrate concrete: placing SACP within the patch appears as a more convenient solution but specific effort should be made to put it in the substrate in order to increase its efficiency when the repair mortar is significantly more resistive than the substrate concrete;
- the interest to remove all the contaminated concrete around the steel is also decisive for a sustainable repair.

Of course, the results provided in this study depend on the selected parameters but the conclusions are expected to remain qualitatively valid if the parameters vary within acceptable ranges.

Finally, and contrary to what is observed with the use of SACP in the maritime field, the relationship between macrocell current (*i.e.* which protects steel) and microcell current (*i.e.* zinc self-corrosion) is very different and far from the ratio 0.9: laboratory testing would be very relevant to approximate a coefficient of efficiency for the concrete sector. This coefficient will be useful to calculate the SACP lifetime because zinc consumption by microcell can only be estimated by autopsy and weighing. It is evident that the electrical resistivity of concrete (which varies according to the environmental conditions) will be the dominant factor.

Acknowledgement

The authors warmly thank all the members of the building-construction commission of CEFRACOR (CEntre FRAnçais de l'AntiCORrosion) and especially the two working groups "Sustainable repairs for reinforced concrete structures" & "Modeling and electrochemical field measurements" for discussions coming from field case studies and feedbacks.

References

References

[1] R Woodward, DW Cullington, AF Daly, PR Vassie, P Haardt, R Kashner, R Astudillo, C Velando, B Godart, C Cremona, et al. Bridge management in europe (brime)-deliverable d14-final report. 2001.

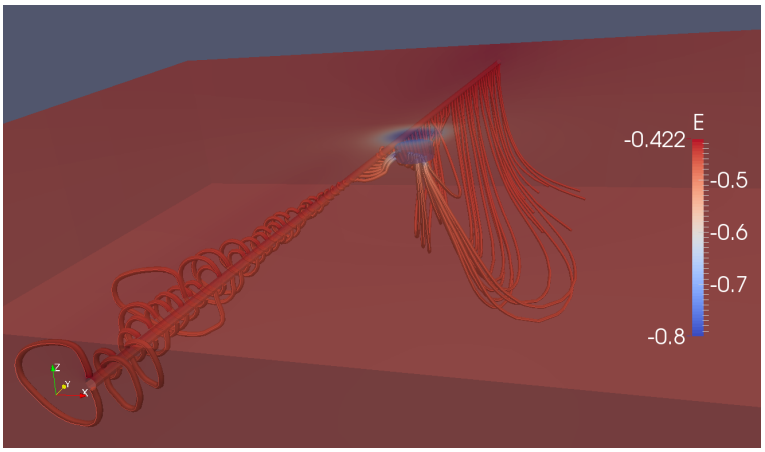

Figure 22: Situation 2 - 3D potential and current lines with a resistivity at 1000 $\Omega.m$ ($V\ vs.\ SCE$)

[2] Kyösti Tuutti. Corrosion of steel in concrete. *Swedish Cement and Concrete Research Institute Stockholm*, 1982.

[3] GP Tilly and Josse Jacobs. *Concrete repairs: Performance in service and current practice*. IHS BRE Press, 2007.

[4] John E Bennett, Caroline Talbot, et al. Extending the life of concrete patch repair with chemically enhanced zinc anodes. In *CORROSION 2002*. NACE International, 2002.

[5] G Sergi and CL Page. Sacrificial anodes for cathodic prevention of reinforcing steel around patch repairs applied to chloride-contaminated concrete. *European Federation of Corrosion Publications(UK)*, 31:93–100, 2000.

[6] M Dugarte, AA Sagüés, and Barranquilla-COLOMBIA Colombia. Modeling performance of galvanic point anodes for cathodic prevention of reinforcing steel in concrete repairs. In *CORROSION 2013*. NACE International, 2013.

[7] Christian Christodoulou, C Goodier, S Austin, John Webb, and Gareth K Glass. Diagnosing the cause of incipient anodes in repaired reinforced concrete structures. *Corrosion Science*, 69:123–129, 2013.

[8] Dale P Barkey. Corrosion of steel reinforcement in concrete adjacent to surface repairs. *ACI Materials Journal*, 101(4):266–272, 2004.

[9] S Soleimani, P Ghods, OB Isgor, and J Zhang. Modeling the kinetics of corrosion in concrete patch repairs and identification of governing parameters. *Cement and Concrete Composites*, 32(5):360–368, 2010.

[10] Shiyuan Qian, Jieying Zhang, and Deyu Qu. Theoretical and experimental study of microcell and macrocell corrosion in patch repairs of concrete structures. *Cement and Concrete Composites*, 28(8):685–695, 2006.

[11] M Raupach. Chloride-induced macrocell corrosion of steel in concrete—theoretical background and practical consequences. *Construction and building materials*, 10(5):329–338, 1996.

[12] B Elsener. Macrocell corrosion of steel in concrete–implications for corrosion monitoring. *Cement and concrete composites*, 24(1):65–72, 2002.

[13] CM Hansson, A Poursaee, and A Laurent. Macrocell and microcell corrosion of steel in ordinary portland cement and high performance concretes. *Cement and Concrete Research*, 36(11):2098–2102, 2006.

[14] Chong Cao, Moe MS Cheung, and Ben YB Chan. Modelling of interaction between corrosion-induced concrete cover crack and steel corrosion rate. *Corrosion science*, 69:97–109, 2013.

[15] Chong Cao and Moe MS Cheung. Non-uniform rust expansion for chloride-induced pitting corrosion in reinforced concrete structures. *Construction and Building Materials*, 51:75–81, 2014.

[16] Tsuyoshi Maruya, Hitoshi Takeda, Kenichi Horiguchi, Satoru Koyama, and Kai-Lin Hsu. Simulation of steel corrosion in concrete based on the model of macro-cell corrosion circuit. *Journal of Advanced Concrete Technology*, 5(3):343–362, 2007.

[17] Sang-Hyo Kim Kim, Ki Yong Ann, et al. Modeling steel corrosion in concrete structures-part 1: A new inverse relation between current density and potential for the cathodic reaction. *International Journal of Electrochemical Science*, 5(3):302–313, 2010.

[18] Chong Cao. 3d simulation of localized steel corrosion in chloride contaminated reinforced concrete. *Construction and Building Materials*, 72:434–443, 2014.

[19] E Lozinguez, J-F Barthélémy, and V Bouteiller. Modelling of patch repair and efficiency of sacrificial anode for cathodic protection. *EUROCORR'16. Montpellier*, 2016.

[20] Stuart Matthews. Conrepnet: Performance-based approach to the remediation of reinforced concrete structures: Achieving durable repaired concrete structures. *Journal of Building Appraisal*, 3(1):6–20, 2007.

[21] J. Costa, M. Restly, and C. Leon. Controlling corrosion on the La Unidad bridge in Campeche. *Concrete Repair Bulletin*, pages 14–16, 2009.

[22] S.F. Daily. Using cathodic protection to control corrosion of reinforced concrete structures in marine environments. *Australasian corrosion association conference*, 1999.

[23] M. Lawson, D. Latham, and B. Kooistra. A concrete cp case study. *Coasts & Ports Australasian Conference*, 2003.

[24] S.R. Sharp, M.C. Brown, and C. Leon. Survey of cathodic protection systems on Virginia bridges. *Virginia Transportation Research Council – research report – Final report VTRC 07-R35*, 2007.

[25] A.A. Sohanghpurwala. Cathodic protection for life extension of existing reinforced concrete bridge elements. a synthesis of highway practice.

National Cooperative Highway Research Program Synthesis 398, 2009.
[26] Christian Christodoulou, CI Goodier, SA Austin, GK Glass, and J Webb. A new arrangement of galvanic anodes for the repair of reinforced concrete structures. *Construction and Building Materials*, 50:300–307, 2014.
[27] Moe MS Cheung and Chong Cao. Application of cathodic protection for controlling macrocell corrosion in chloride contaminated reinforced concrete structures. *Construction and Building Materials*, 45:199–207, 2013.
[28] JLS Ribeiro, Z Panossian, and SMS Selmo. Proposed criterion to assess the electrochemical behavior of carbon steel reinforcements under corrosion in carbonated concrete structures after patch repairs. *Construction and Building Materials*, 40:40–49, 2013.
[29] SC Kranc and Alberto A Sagüés. Detailed modeling of corrosion macrocells on steel reinforcing in concrete. *Corrosion Science*, 43(7):1355–1372, 2001.
[30] RN Cox, R Cigna, Ø Vennesland, and T Valente. Corrosion and protection of metals in contact with concrete. *Final Report, EUR*, 17608, 1997.
[31] C ASTM. 876-91 (reapproved 1999),"standard test method for half-cell potentials of uncoated reinforcing steel in concrete". In *American Society for Testing and Materials*, pages 461–466, 1999.
[32] RILEM TC, C Andrade EMC, C Alonso, J Gulikers, RB Polder, R Cigna, Ø Vennesland, and M Salta. Recommendations of rilem tc-154-emc:" electrochemical techniques for measuring metallic corrosion". *Materials and Structures*, 37:623–643, 2004.
[33] Dieter Landolt. *Corrosion and surface chemistry of metals*. CRC Press, 2007.
[34] GK Glass, AM Hassanein, and NR Buenfeld. Monitoring the passivation of steel in concrete induced by cathodic protection. *Corrosion science*, 39(8):1451–1458, 1997.
[35] AM Hassanein, GK Glass, and NR Buenfeld. Protection current distribution in reinforced concrete cathodic protection systems. *Cement and Concrete Composites*, 24(1):159–167, 2002.
[36] Bo Yu, LuFeng Yang, Ming Wu, and Bing Li. Practical model for predicting corrosion rate of steel reinforcement in concrete structures. *Construction and Building Materials*, 54:385–401, 2014.
[37] M Saleem, M Shameem, SE Hussain, and M Maslehuddin. Effect of moisture, chloride and sulphate contamination on the electrical resistivity of portland cement concrete. *Construction and Building Materials*, 10(3):209–214, 1996.
[38] T Liu and RW Weyers. Modeling the dynamic corrosion process in chloride contaminated concrete structures. *Cement and Concrete Research*, 28(3):365–379, 1998.
[39] EN ISO. 12696: 2000, cathodic protection of steel in concrete. *British Standards Institution, London*, 2000.
[40] S Laurens, P Hénocq, N Rouleau, F Deby, E Samson, J Marchand, and B Bissonnette. Steady-state polarization response of chloride-induced macrocell corrosion systems in steel reinforced concrete—numerical and experimental investigations. *Cement and Concrete Research*, 79:272–290, 2016.
[41] Getfem++. `http://www.download.gna.org/getfem/htlm/homepage`.
[42] Christophe Geuzaine and Jean-François Remacle. Gmsh: A 3-d finite element mesh generator with built-in pre-and post-processing facilities. *International Journal for Numerical Methods in Engineering*, 79(11):1309–1331, 2009.
[43] Amy Henderson Squillacote and James Ahrens. *The paraview guide*, volume 366. Kitware, 2007.
[44] RB Polder, WHA Peelen, F Lollini, E Redaelli, and L Bertolini. Numerical design for cathodic protection systems for concrete. *Materials and corrosion*, 60(2):130–136, 2009.